GEOLOGICA CARPATHICA, AUGUST 2022, 73, 4, 353–363 https://doi.org/10.31577/GeolCarp.73.4.4

Short Communication

Metamorphism of the westernmost Triassic metasedimentary rocks in the Sakar Unit, Sakar–Strandja Zone, Bulgaria

TZVETOMILA VLADINOVA[1,✉] and MILENA GEORGIEVA[2]

[1]Geological Institute, Bulgarian Academy of Sciences, Department of Geochemistry and Petrography, Acad.G.Bonchev str., 1113 Sofia Bulgaria; ✉tz.vladinova@gmail.com
[2]Sofia University "St. Kliment Ohridski", Departament of Mineralogy, Petrology and Economic Geology, 15 Tsar Osvoboditel Blvd., 1504 Sofia, Bulgaria; milena@gea.uni-sofia.bg

(Manuscript received May 16, 2022; accepted in revised form August 24, 2022; Associate Editor: Marian Janák)

Abstract: Metasedimentary sequence from the westernmost Sakar Unit (Klokotnitsa Village area), Sakar–Strandja Zone, comprises a variety of lithologies with Triassic protolith age. In the study area, the Sakar Unit is affected by low-grade metamorphism in the frame of the Maritsa dextral strike-slip shear zone and separates two first-order units of the Balkan orogenic system – the Rhodope massif and the Srednogorie Zone. We present the petrography, mineral chemical data, and thermodynamic modelling of metasediments for a better understanding of the protoliths origin and metamorphic evolution. The mineral assemblages in Triassic metasediments suggest sedimentary protoliths containing quartz, clay, and carbonate minerals (sandstones, clays, and limestones). The detrital minerals (quartz, albite, orthoclase and accessory phases – zircon, monazite, apatite) reveal potential granite source provenance. The dominance of phengite–chlorite association correlates with low temperature and water-saturated conditions. The Perple_X pseudosection, combined with modelled mineral assemblages and mineral chemistry isopleths of muscovite and chlorite, correspond to metamorphism in the range 275–330 °C and 3–4 kbar. The results correspond with a chlorite geothermometer. The thermodynamic modelling corroborates the petrographic observations and proves greenschist metamorphic conditions that affected the Triassic sedimentary cover of the westernmost Sakar Unit.

Keywords: Sakar–Strandja Zone, Sakar Unit, metasedimentary rocks, petrography, mineral chemistry, Perple_X modelling

Introduction

The Sakar–Strandja Zone (SSZ; Dimitrov 1958; Ivanov 2017) occupies a large area in southeast Bulgaria and European Turkey. The SSZ is accepted as Variscan (Hercynian) orogeny, affected by Late Jurassic to Early Cretaceous greenschist–amphibolite-facies metamorphism (e.g., Vladinova et al. 2019; Bonev et al. 2020), which is a product of Early Alpine/Cimmerian orogenesis (e.g., Gerdjikov 2005; Cattò et al. 2017). The regional geological setting of the SSZ is controversial. It is referred to the East Srednogorie Unit (Dabovski et al. 2002) or the Srednogorie Zone (Dabovski & Zagorchev 2009; Zagorchev 2020), where metamorphites of the SSZ and Central and Ihtiman Sredna Gora represent the pre-Cretaceous crystalline basement. On the other hand, Schmid et al. (2020) consider the SSZ as a lateral equivalent of the Circum-Rhodope Belt based on the close kinematics, degree, and age of metamorphism. The present study, however, accepts the SSZ as an independent tectonic zone (Gerdjikov 2005; Machev et al. 2015; Bonev et al. 2019), which is part of the inner Balkanides (Ivanov 2017). In many places, the SSZ rocks are unconformably covered by Cretaceous sedimentary and volcanic rocks, as well as Eocene–Oligocene sediments of the Thrace Basin (Ivanov 2017; Okay et al. 2001). The two units which comprise the SSZ, the Sakar and Strandja, differ both in their tectonic evolution and metamorphic grade (Ivanov 2017). The Triassic age of the Sakar Unit metasediments is determined by fossils (Chatalov 1990), and previous studies described a regional metamorphic gradient with conditions increasing from the west to the east, from greenschist to amphibolite facies. The Strandja Unit differs in presence of Jurassic metasediments, Alpine allochthonous units, numerous intrusive and volcanic Cretaceous rocks, and lower metamorphic grade (anchimetamorphism to greenschist facies).

The metasediments in the western parts of the Sakar Unit (to the south of the town of Simeonovgrad and in the vicinities of the villages of Klokotnitsa and Krepost, Fig.1) were not studied in detail by Chatalov (1990), however, their Triassic age and similar lithology correlated them to the Sakar Type Triassic, which is defined in the eastern Topolovgrad area. Boyanov et al. (1992) correlated these western Sakar Unit metasediments to the Ustrem and Srem formations in the Topolovgrad area and recently, they were assigned by Zagorchev & Budurov (2009) to the Triassic terrigenous-carbonate association of the Sakar type. The biostratigraphic data and U–Pb detritial zircons ages reveal their similar Early Devonian–

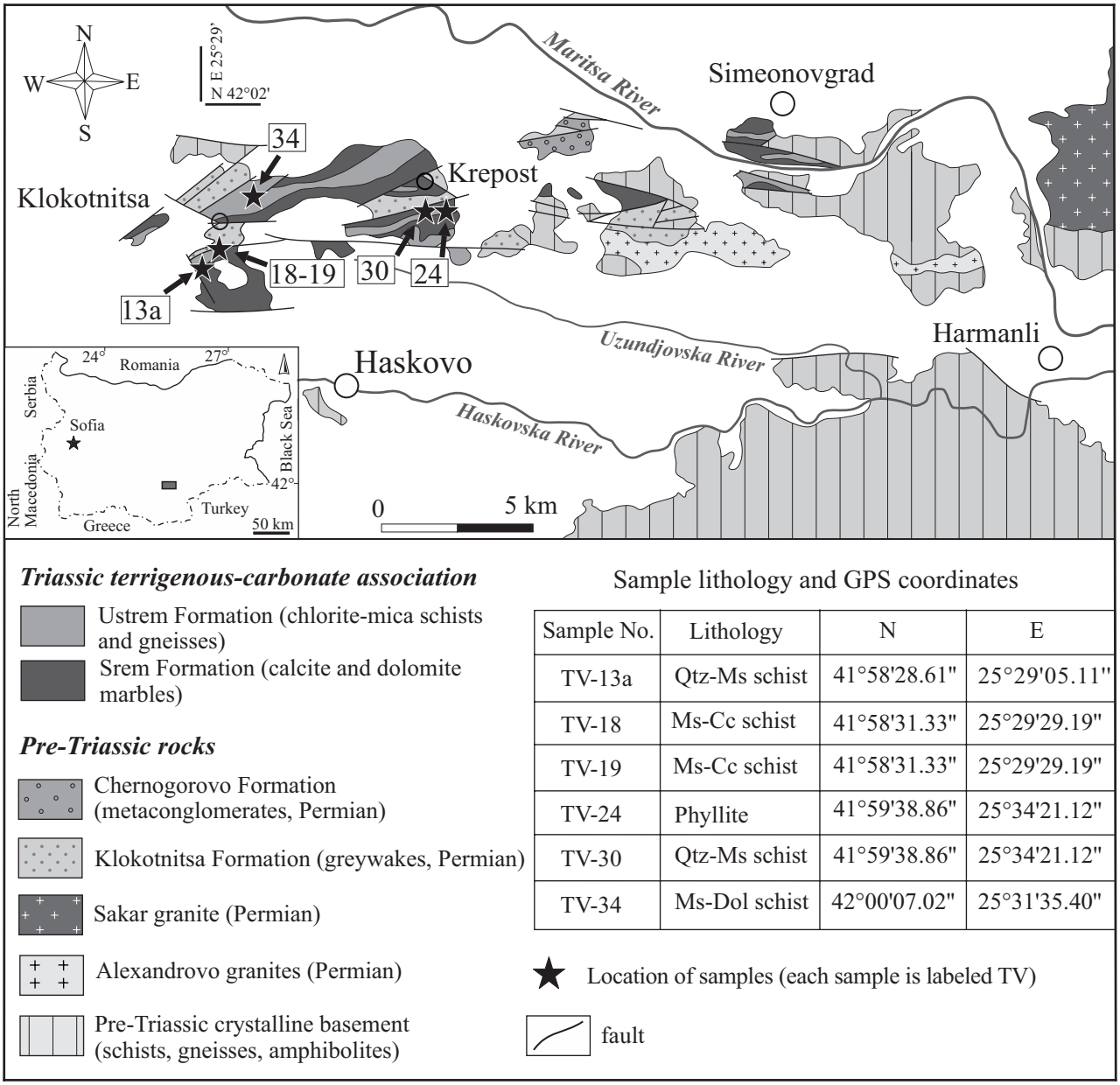

Sample No.	Lithology	N	E
TV-13a	Qtz-Ms schist	41°58'28.61"	25°29'05.11"
TV-18	Ms-Cc schist	41°58'31.33"	25°29'29.19"
TV-19	Ms-Cc schist	41°58'31.33"	25°29'29.19"
TV-24	Phyllite	41°59'38.86"	25°34'21.12"
TV-30	Qtz-Ms schist	41°59'38.86"	25°34'21.12"
TV-34	Ms-Dol schist	42°00'07.02"	25°31'35.40"

Fig. 1. Simplified geological map of the westernmost Triassic metasedimentary rocks in the Sakar Unit, Sakar–Strandja Zone, compiled according to Boyanov et al. (1989, 1990, 1991) with a table of sample lithology and GPS coordinates. The location of the investigated area (Sakar Unit) in SE Bulgaria is shown in the box area.

Middle Triassic sedimentation time (Chatalov 1990; Vladinova et al. 2017, 2018; Filipov et al. 2018). Scarce outcrops and a more complex geology in the western Sakar Unit, which has numerous folds and faults, prevent the correct interpretation of field relations and systematic rock sampling. In the study area, the metasediments have a lower thickness, which could reflect a different sediment source area and setting of deposition. The reason for the regional gradient in the Sakar Unit is disputable. Lower metamorphic grade in this area was deduced from field observations and petrography (Kozhoukharov et al. 1968); however, modern metamorphic studies are lacking. Some authors connected the post-Triassic metamorphic event with the intrusion of Sakar and Aleksandrovo granites (Kozhoukharov et al. 1968; Ivanov 2017); however, their Carboniferous–Permian (330–300 Ma) age was recently proven by U–Pb zircon geochronology (Machev et al. 2015; Peytcheva et al. 2016; Bonev et al. 2019; Pristavova et al. 2019). The presence of younger Permian–Triassic granitoids provoked the division of two magmatic events: (1) Late Carboniferous (312–295 Ma) and (2) Permian–Triassic (275–230 Ma) related to the fragment separation of the southern Laurusia edge (Sałacińska et al. 2021). In contrast, Bonev et

al. (2021) interpreted it as continuous Paleotethys subduction, which produced a Permian magmatic arc with subsequent formation of the Permian–Triassic arc basin. This scenario is supported by the presence of the Permian–Triassic metasedimentary sequence deposited in the formed arc basin (Aysal et al. 2018). The extensive Carboniferous–Permian plutonism is a prerequisite for the emergence of high-grade metamorphism (Vladinova & Georgieva 2020; Sałacińska et al. 2022). It is obvious that the western outcrops are more intensively affected by deformation in the frame of the large tectonic dislocation in the area – the Maritza shear zone (Kozhoukharov et al. 1968). This poses the question: is the lower-grade metamorphism observed in the metasediments imposed on higher-grade mineral associations?

In this study, we provide more information on the petrography and mineral chemistry of metasediments and apply an up-to-date approach in order to characterize the metamorphic conditions using Perple_X modelling and geothermometers based on the chemical composition of metamorphic minerals. Giving quantitative parameters of metamorphism in the area will help for a better understanding of the evolution of the SSZ, and thus will be useful for further tectono-metamorphic scenarios.

Materials and methods

We studied the petrography, mineral chemistry, and bulk rock composition of six samples of metasediments from the western Sakar Unit (outcrops of Triassic sediments to the west of Sakar granite). The sample location and GPS coordinates are shown in Figure 1. Carbonate rocks (calcite, dolomite- and impure marbles) alternate with less common silicate–carbonate schists (muscovite–calcite and quartz–muscovite schists). The carbonate–silicate schists (Fig. 2a) are composed of muscovite and calcite layers and alternate with fine-grained and cataclased phyllites (Fig. 2b). The alternation between carbonate–silicate schists and impure marble marks the appearance of massive marble layers (Fig. 2c). The silicate rocks are sampled in single outcrops with unclear relations to the surrounding rocks (Fig. 2d). They are composed mainly of phyllosilicates and quartz bands that trace the foliation.

The chemical mineral analysis was carried out with a JEOL Superprobe-733 electron microprobe at the Geological Institute, the Bulgarian Academy of Sciences (Sofia, Bulgaria), SEM Jeol JSM-259 6610 LV at the University of Belgrade (Serbia), and FEI 200 SEM with EDAX-EDS detector at the University of Cagliari (Italy). The P–T pseudo-sections were

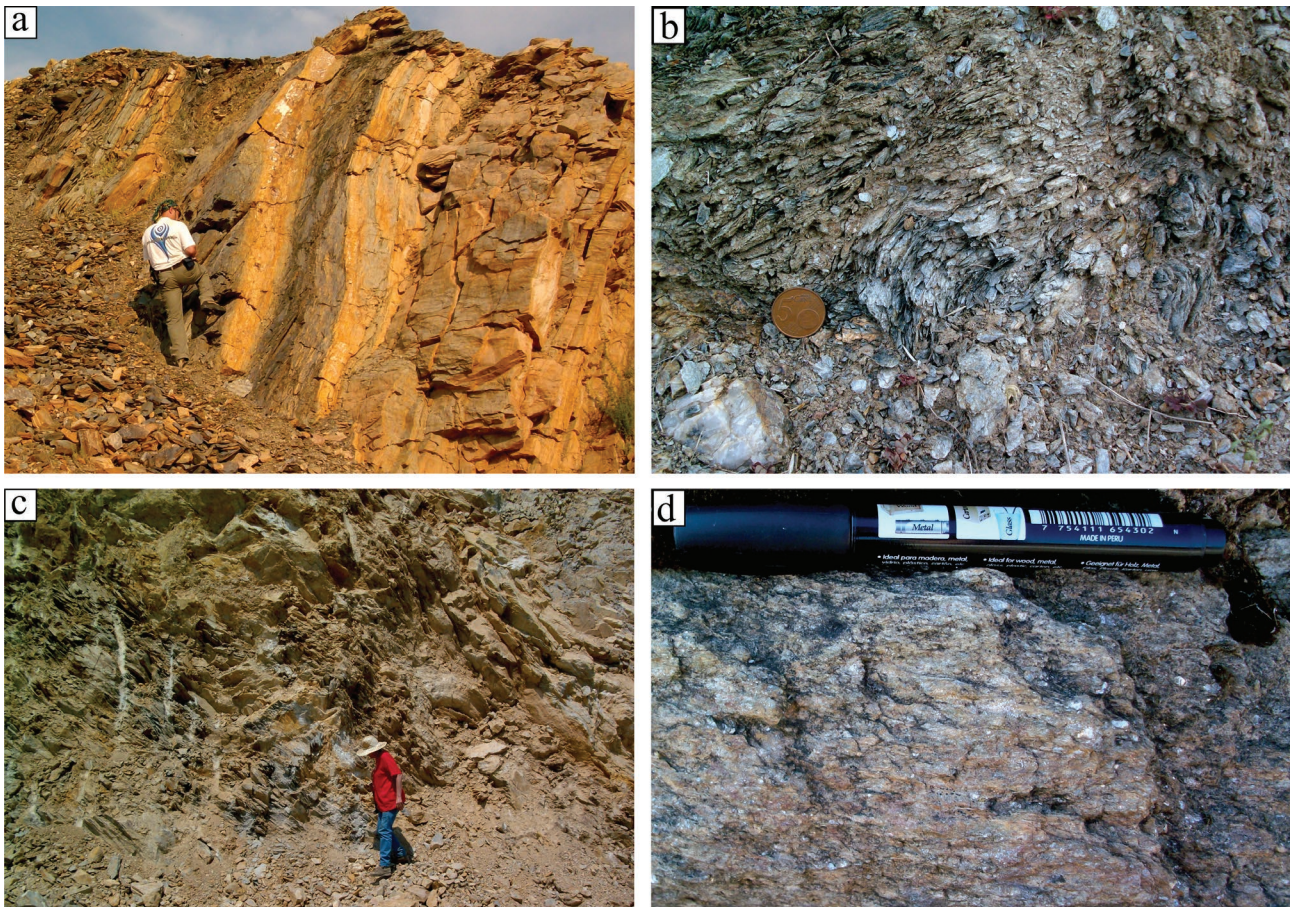

Fig. 2. Field photographs of the metasedimentary succession: **a** — Alternation of carbonate-silicate rocks and phyllites (TV-24); **b** — Cataclased phyllites with numerous of folds (TV-24); **c** — Alternation between carbonate–silicate (TV-34) and carbonate rocks; **d** — Single outcrops of silicate rocks (TV-30).

calculated for the carbonate–silicate sample (TV-24), using the bulk rock composition determined by wet chemical analysis and carbonate analysis at the Chemical laboratory at the University of Sofia.

Petrography

The metasediments in the studied area show a wide range in composition from carbonate (calcite and dolomite marbles) to carbonate–silicate rocks (muscovite–calcite schists and impure marbles) and siliciclastic metasediments (quartz–muscovite, quartz–muscovite–chlorite schists, etc.), according to the classification of Rosen et al. (2007).

Siliciclastic metasediments (TV-13a, TV-30) are less common in the area. The pronounced foliation in these rocks is defined by phyllosilicates (muscovite, ± chlorite) (Fig. 3a–c), while the deformation in quartz-dominated bands and lenses is obliterated by static recrystallization. Rounded to subangular plagioclase porphyroclasts show partially recrystallized and resorbed rims (Fig. 3a). Along with the porphyroclasts, calcite, hematite, and barite were deposited during weathering and sedimentation in an oxidizing environment while later, recrystallization at a higher temperature healed the fractures. Fragments, as well as rounded to euhedral grains of detrital accessory minerals (rutile, zircon, titanite, monazite, apatite) are unevenly distributed in the samples and often clustered together (Fig. 3b, c). Numerous small opaque minerals in the matrix define the foliation in mica-rich samples, while only magnetite forms large, euhedral syn- to post-kinematic crystals. Non-stoichiometric Al_2O_3–SiO_2–H_2O kaolinite like alumosilicate fills the space among muscovite flakes in sample TV-13a, which appears to be of relict origin rather than a product of post-metamorphic weathering.

The carbonate–silicate rock (containing between 5 % and 50 % carbonate minerals, according to Rosen et al. 2007) is composed mainly of phyllosilicate minerals, which were recognized as phyllite in the field (Fig. 2a, b; TV-24). Along with muscovite and chlorite, quartz, calcite and albite are present in the fine-grained matrix. Calcite, chlorite, and muscovite also form larger syn-kinematic grains (Fig. 3d). Accessory phases are allanite, apatite, pyrite and chalcopyrite, but ilmenite is the most abundant and forms anhedral to enlongated subhedral grains that envelope and replace single rutile grains. The sample shows a prominent crenulation cleavage (Fig. 3d) with oblique or sub-horizontal S_1 foliation, which is defined by matrix minerals and superposed sub-vertical S_2 foliation by fine-grained phyllosilicates and rare ilmenite, thereby reflecting the complex deformation history of the area.

Impure marbles (containing between 50 % and 95 % carbonate minerals, Rosen et al. 2007) are composed of elongate to isometric calcite grains with varying size (TV-18, TV-19, TV-34). In some samples, the main silicate mineral is quartz, while in others, muscovite-chlorite bands are abundant and define the rock foliation along with calcite. In samples with stronger foliation, the silicate bands are finer grained in comparison to coarser carbonate lenses. Subangular quartz and plagioclase are recrystallized and form triple junctions. Magmatic twining in plagioclases is almost completely obliterated. Along with matrix calcite, larger subhedral calcite porphyroclasts with rims and cracks, which are enveloped and filled with iron oxides, are present (Fig. 3e). Similar calcite grains were described by Chatalov (1990) as crinoid bioclast, and these single crystals are more resistant to diagenesis and metamorphism, but change their composition and exsolve Fe as well. The sub-rhombohedral forms can be inherited also from dolomite crystals, which during metamorphic dedolomitization processes, exsolve Fe. Similar calcite examples can be found in the research by Vandeginste & John (2012) and Makhloufi & Samankassou (2019). Dolomite is present only in sample TV-34, where it is the main carbonate mineral, and K-feldspar porphyroclasts (Fig. 3f) dominate over plagioclase. In the foliated matrix, dolomite forms elongated grains and associates with feldspars and quartz, while larger, dusty subhedral dolomite grains form carbonate lenses (Fig. 3f).

In the studied metasediments, we observed relatively simple mineralogy, but high variation in mineral modal composition. All samples have well-developed pervasive foliation defined mainly by phylosilicates with intensive recovery of calcite, quartz, and plagioclase. Detrital accessory minerals are more abundant in the siliciclastic and carbonate–silicate samples, while only some opaque minerals form during metamorphism.

Mineral chemistry

The structural formulae of muscovite were calculated on the basis of 11 oxygen atoms (Table 1). Dioctahedral mica have multiple compositional substitutions and show significant heterogeneity in diagenetic to very low metamorphic conditions, especially for the illitic component (Abad et al. 2006). In the studied samples, the illitic substitution is insignificant (Fig. 4a); however, the phengite content varies among samples (3.19–3.46 Si apfu). Phengitic substitution reflects a positive correlation between Fe+Mg and Si (with highest values for muscovites from siliciclastic sample TV-13a) and negative correlations between Al and Fe+Mg or Al and Si (Fig. 4b). The aluminum content in muscovite is controlled not only by phengitic substitution, but also by rock composition. The carbonate–silicate sample (TV-24) with abundant chlorite and muscovite shows the highest Al_{tot} content as well. For each sample, the heterogeneity in muscovite composition is negligible, reflecting the achieved equilibrium at low-grade metamorphic conditions. Chlorites were analysed in 3 samples (TV-18, TV-24 and TV-30) and structural formulae were calculated on the basis of 14 oxygen atoms (Table 2). Chlorites from impure marble (TV-18) and carbonate-bearing phyllite (TV-24), however, do not meet the constraints of Vidal et al. (2001) and have $K + Na + Ca > 0.05$ apfu, thus indicating possible interlayering with other sheet silicates, which is a common feature in fine-grained low-metamorphic rocks. According to

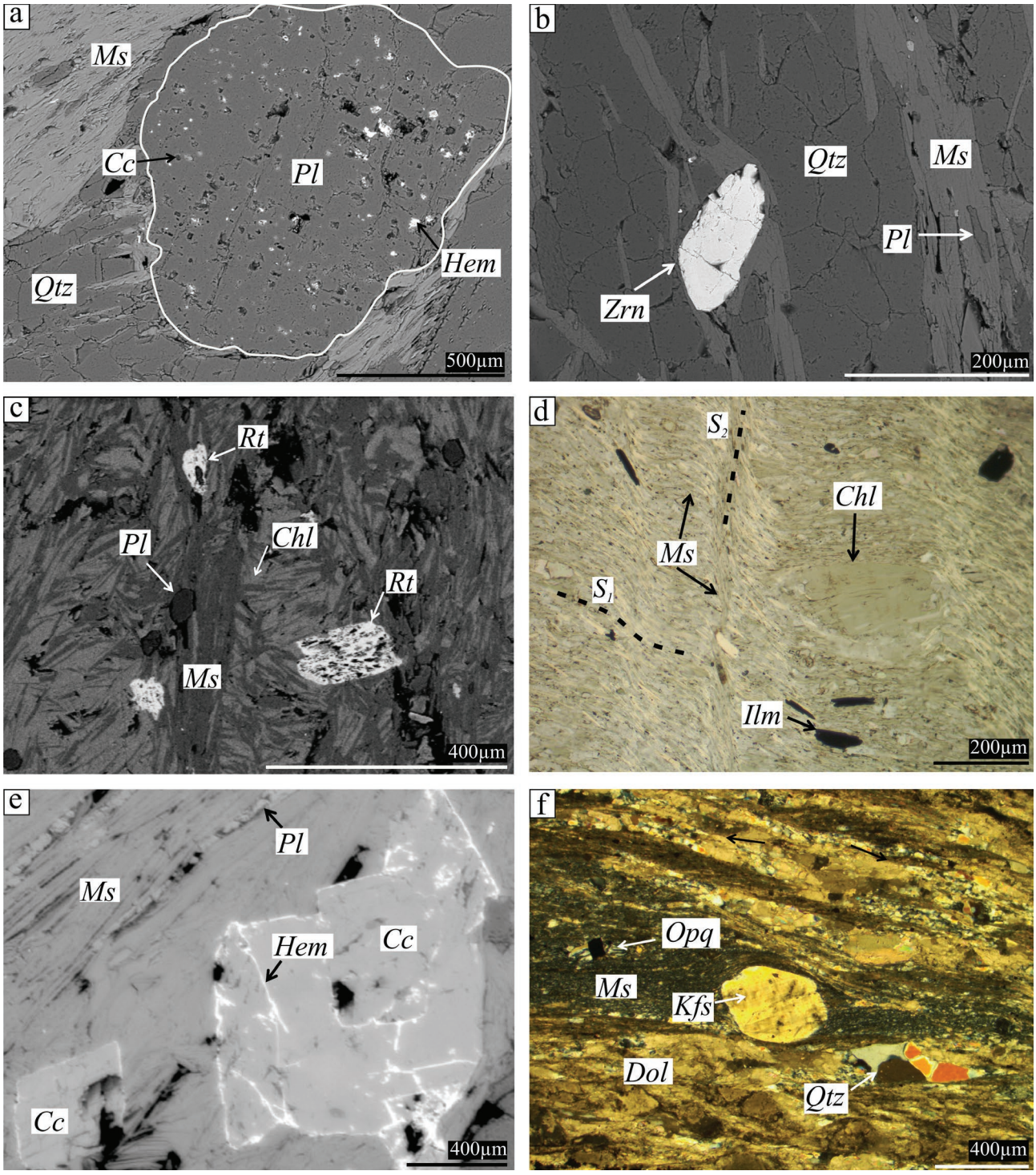

Fig. 3. Photomicrographs of the studied samples: **a** — Plagioclase clast with calcite, hematite, and barite inclusions in quartz–muscovite schist (BSE image, TV-13a); **b** — Subhedral zircon grain in muscovite matrix of quartz-muscovite schist (BSE and CPL images, TV-13a); **c** — Subhedral to rounded rutile grains in the muscovite–chlorite matrix of muscovite–chlorite schist (BSE image, TV-30); **d** — Syn-kinematic chlorite flake in a fine-grained muscovite–chlorite–calcite matrix of phyllite (PPL, TV-24); **e** — Calcite porphyroblasts enveloped in Fe oxides in the muscovite matrix of muscovite–calcite schist (BSE image, TV-19); **f** — Rounded K-feldspar clast in the muscovite band in muscovite–dolomite schist (CPL, TV-34). Mineral abbreviations: Pl – plagioclase, Qtz – quartz, Ms – muscovite, Cc – calcite, Hem – hematite, Zrn – zircon, Ilm – ilmentine, Dol – dolomite, Kfs – K-feldspar, Opq – opaque mineral.

Table 1: Representative muscovite analyses and structural formulae on the basis of 11 oxygen atoms from metasediments of the western Sakar Unit.

	TV-13a	TV-13a	TV-13a	TV-18*	TV-19	TV-19	TV-19	TV-24	TV-24	TV-24	TV-34	TV-34	TV-34
SiO_2	48.71	48.55	47.72	50.34	47.55	48.69	47.91	46.71	48.26	48.09	51.10	50.86	50.55
Al_2O_3	26.32	25.72	26.81	33.19	28.22	28.04	28.44	31.68	32.14	31.55	25.62	26.48	26.24
MgO	3.02	3.33	2.99	3.33	2.48	2.72	2.30	1.79	1.36	1.63	4.24	4.34	4.20
FeO	6.34	6.75	6.12	1.57	4.70	4.44	4.31	2.90	2.30	2.71	0.59	0.78	0.80
K_2O	11.23	11.02	10.54	10.73	10.50	10.74	10.42	8.88	10.41	10.04	10.75	10.98	10.42
Na_2O	0.00	0.00	0.00	0.24	0.52	0.43	0.53	0.39	0.42	0.27	0.00	0.28	0.35
MnO	0.00	0.00	0.00	0.00	0.06	0.03	0.04	0.00	0.02	0.04	0.13	0.06	0.00
CaO	0.00	0.00	0.00	0.00	0.19	0.05	0.26	0.10	0.03	0.13	0.09	0.07	0.08
TiO_2	0.65	0.00	0.54	0.59	0.24	0.21	0.69	0.45	0.49	0.32	0.88	0.42	0.98
Total	96.27	95.37	94.72	99.99	94.46	95.35	94.90	92.90	95.43	94.78	93.40	94.27	93.62
Si	3.31	3.33	3.28	3.19	3.26	3.30	3.26	3.19	3.22	3.23	3.46	3.42	3.41
Al^{IV}	0.69	0.67	0.72	0.81	0.74	0.70	0.74	0.82	0.79	0.77	0.55	0.58	0.59
Sum T	4.00	4.00	4.00	4.00	4.00	4.00	4.00	4.00	4.00	4.00	4.00	4.00	4.00
Al^{VI}	1.42	1.41	1.46	1.67	1.54	1.54	1.54	1.73	1.74	1.72	1.50	1.52	1.50
Mg	0.31	0.34	0.31	0.32	0.25	0.28	0.23	0.18	0.14	0.16	0.43	0.44	0.42
Fe^{2+}	0.36	0.39	0.35	0.08	0.27	0.25	0.25	0.17	0.13	0.15	0.03	0.04	0.05
Mn	0.00	0.00	0.00	0.00	0.00	0.00	0.00	0.00	0.00	0.00	0.01	0.00	0.00
Ti	0.03	0.00	0.03	0.03	0.01	0.01	0.04	0.02	0.03	0.02	0.05	0.02	0.05
Sum O	2.12	2.14	2.14	2.10	2.08	2.08	2.06	2.10	2.03	2.05	2.01	2.02	2.02
K	0.97	0.97	0.93	0.87	0.92	0.93	0.91	0.77	0.89	0.86	0.93	0.94	0.90
Na	0.00	0.00	0.00	0.03	0.07	0.06	0.07	0.05	0.05	0.04	0.00	0.04	0.05
Ca	0.00	0.00	0.00	0.00	0.01	0.00	0.02	0.01	0.00	0.01	0.01	0.01	0.01
Sum A	0.97	0.97	0.93	0.90	1.00	0.99	0.99	0.83	0.94	0.90	0.93	0.98	0.95
XMg	0.46	0.47	0.47	0.79	0.48	0.52	0.49	0.52	0.51	0.52	0.93	0.91	0.90
$Mg+Fe^{2+}$	0.67	0.73	0.66	0.40	0.52	0.53	0.48	0.35	0.26	0.32	0.46	0.48	0.47
Al tot	2.11	2.08	2.17	2.48	2.28	2.24	2.28	2.55	2.52	2.49	2.04	2.10	2.09

* analyses on water-free basis

the Si–R^{2+} diagram of Jiang et al. (1994), the possible contamination is from illite, kaolinite, or muscovite, and this contamination affects the Al content used in thermometry. For chlorites from these two samples, the other constraint, $(Al^{VI}–Al^{IV})/2=6$ – octahedral cation sum is not fulfilled. Except for contamination, this discrepancy could be explained by the presence of Fe^{3+} and not by pure di-trioctahedral substitution. XFe ($Fe_{tot}/Fe_{tot}+Mg$) is in the range of 0.24 to 0.54, with lowest values in impure marble (TV-18). Despite the variation in composition and XFe, all analyzed chlorites fall in the ripidolite field according to the Hey (1954) classification diagram (Fig. 4c). In the triangle $(Al+□)-Mg-Fe$ diagram of Zane & Weiss (1998), the studied chlorites plot in the field of Type I Mg–Fe trioctahedral chlorites. With lower XFe (0.24–0.25, sample TV-18), chlorites from impure marble plot in the field of Mg-chlorites, while the other analyses plot close to the border of Mg- to Fe-chlorites. The Si content (<3 apfu) is lower than what was observed in low-temperature diagenetic systems, and together with Fe, Mg and high Al^{IV} (>1.25 apfu), indicates greenschist facies metamorphism (Fig. 4d). Despite the different structural position, in the fine-grained matrix or larger syn-kinematic flakes (e.g., sample TV-24), the chlorite composition is rather uniform for each sample. Plagioclase is the most common feldspar in the studied samples (TV-13a and TV-24), while K-feldspar dominates only in sample TV-34. Structural formulae were calculated on the basis of 8 oxygen atoms and are listed in Table 3. In all four samples analyzed, the plagioclase is albite ($An_{0–2}$), regardless of the size and structural position (cores and rims of bigger grains with clastic origin or smaller grains in the matrix). Plagioclase porphyroclasts in quartz–muscovite schists (TV-13a) show partially recrystallized rims and cores that preserve a foliation oblique to the rock matrix foliation (Fig. 3a). It appears that their composition was originally albitic or had been completely reset during weathering, sedimentation, and low-grade metamorphism.

K-feldspar ($Or_{94–99}$) is abundant only in dolomite impure marble (sample TV-34), with the highest albite content (Ab_5) for K-feldspar in the matrix that together with dolomite form foliation.

Thermobarometry

Chlorite is a common mineral in low grade metamorphic rocks, and its composition was successfully used to estimate the temperature of diagenetic, hydrothermal, and low-temperature metamorphic systems (Bourdelle 2021). In the studied samples, chlorite is a common mineral that defines the rocks matrix foliation and shows rather uniform composition. We applied the empirical equation of Cathelineau (1988) based on the Al^{IV} content only to chlorites from sample TV-30, which fulfill the constraints given by Vidal et al. (2001) and did not show contamination. Obtained temperatures correspond to greenschist facies in the range 320–330 °C. By using the substitution Si–R^{2+} (R^{2+} – divalent cations),

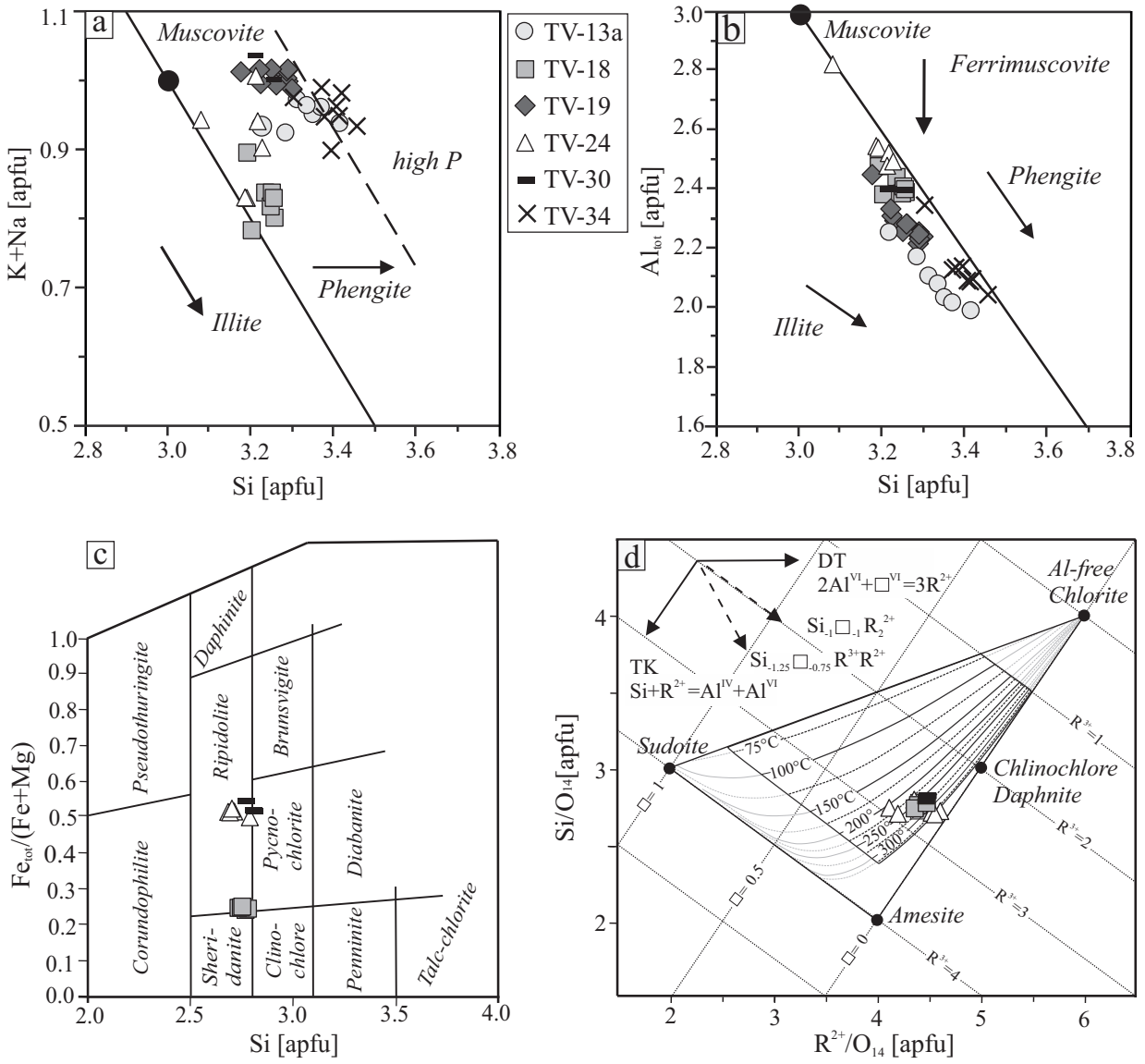

Fig. 4. Classification and composition diagrams of rock-forming minerals: **a** — Si (apfu) vs K+Na (apfu) diagram with main substitutions in white micas according to Abad et al. (2006); **b** — Negative correlations between Si (apfu) and Al (apfu) in white micas, reflecting the phengitic substitution according to Abad et al. (2006); **c** — Chlorite classification by Hey (1954); **d** — Semi-empirical graphical thermometer of Bourdelle & Cathelineau (2015), R^{2+} – divalent cations (Fe^{2+} and Mg^{2+}); R^{3+} – trivalent cations (Al^{3+} and Fe^{3+}); □ – vacancies.

the values from the semi-empirical graphical thermometer of Bourdelle & Cathelineau (2015) for the same sample are lower, in the range 250–275 °C (Fig. 4d). Application of Si in the phengite barometer of Massonne & Schreyer (1987) shows significant scatter in estimated pressure (3–10 kbar), and most of the samples do not meet the requirement for the coexistence of phlogopite and K-feldspar.

Thermodynamic modelling

In order to constrain the P–T conditions further, we applied thermodynamic modelling using the software package Perple_X (Connolly 1990), version 6.8.8. The bulk composition of carbonate-bearing phyllite (TV-24) was normalized to 100 % after disregarding P_2O_5 (mostly contained in apatite) and MnO in minor content. TiO_2 was also excluded from calculation, since it is present mainly in accessory phases as rutile and ilmenite. It appears that rutile is of detrital origin and is found mainly as inclusion in ilmenite; thus, the two minerals are far from equilibrium. The compositional space is K_2O–Na_2O–CaO–FeO–MgO–Al_2O_3–SiO_2–H_2O–CO_2 (KNCFMASH–CO_2) and the calculated composition is given in Figure 5. The P–T pseudo-section is for fluid-saturated conditions, and XCO_2 in fluid was set to 0.39, taking the calculated CO_2 from carbonate analysis (soluble in 5 % HCl) as part of LOI of the bulk sample. Total iron was considered ferrous, because the main iron-rich mineral chlorite contains minor ferric iron.

Table 2: Representative chlorite analyses and structural formulae on the basis of 14 oxygen atoms from metasediments of the western Sakar Unit.

	TV-18*	TV-18*	TV-18*	TV-24	TV-24	TV-24	TV-24	TV-30	TV-30	TV-30
SiO_2	32.18	31.84	31.95	25.44	25.72	25.12	26.58	25.65	25.04	25.48
Al_2O_3	25.99	26.45	26.62	20.75	21.43	21.11	21.67	20.46	19.66	19.87
MgO	26.51	26.01	25.69	14.04	14.22	13.46	13.94	12.71	12.89	13.20
FeO	15.09	15.37	15.33	26.70	26.77	26.39	24.90	26.80	24.74	25.13
MnO	0.00	0.00	0.00	0.13	0.15	0.00	0.00	0.43	0.00	0.00
CaO	0.23	0.33	0.40	0.00	0.02	0.05	0.02	0.00	0.00	0.00
Na_2O	0.00	0.00	0.00	0.24	0.17	0.19	0.03	0.00	0.00	0.00
K_2O	0.00	0.00	0.00	0.00	0.13	0.23	0.43	0.00	0.00	0.00
TiO_2	0.00	0.00	0.00	0.06	0.26	0.04	0.04	0.00	0.00	0.00
Total	100.00	100.00	99.99	87.36	88.87	86.59	87.61	86.05	82.33	83.68
Si	2.77	2.74	2.75	2.71	2.69	2.70	2.79	2.78	2.81	2.81
Al^{IV}	1.23	1.26	1.25	1.29	1.31	1.30	1.21	1.22	1.19	1.19
Sum T	4.00	4.00	4.00	4.00	4.00	4.00	4.00	4.00	4.00	4.00
Al^{VI}	1.41	1.43	1.46	1.32	1.34	1.38	1.47	1.39	1.41	1.40
Ti	0.00	0.00	0.00	0.01	0.02	0.00	0.00	0.00	0.00	0.00
Fe^{2+}	1.09	1.11	1.10	2.38	2.34	2.37	2.18	2.43	2.32	2.32
Mn	0.00	0.00	0.00	0.01	0.01	0.00	0.00	0.04	0.00	0.00
Mg	3.40	3.34	3.30	2.23	2.22	2.16	2.18	2.05	2.16	2.17
Sum O	5.89	5.88	5.86	5.95	5.94	5.91	5.83	5.91	5.89	5.89
Ca	0.02	0.03	0.04	0.00	0.00	0.01	0.00	0.00	0.00	0.00
Na	0.00	0.00	0.00	0.05	0.04	0.04	0.01	0.00	0.00	0.00
K	0.00	0.00	0.00	0.00	0.02	0.03	0.06	0.00	0.00	0.00
Sum A	0.06	0.03	0.04	0.05	0.06	0.08	0.07	0.00	0.00	0.00
Fe+Mg	4.37	4.45	4.40	4.62	4.56	4.53	4.36	4.48	4.48	4.49
XFe	0.25	0.25	0.25	0.52	0.51	0.52	0.50	0.54	0.52	0.52
Al tot	2.74	2.69	2.70	2.61	2.65	2.68	2.68	2.61	2.60	2.59

* analyses on water-free basis

The thermodynamic database used was the updated hp02ver.dat, with the activity-composition models for the white mica and chlorite of Holland & Powell (1998). Calcite and plagioclase were considered pure phases.

On the phase diagram, the field of the muscovite–paragonite–chlorite–albite–calcite–quartz association is closer to the mineral composition of the rock (albite–carbonate–chlorite–muscovite–quartz). This paragenesis is stable over the range of 250 to 450 °C, as well as in the lower pressure part of the diagram (3.5 to 5 kbar). According to the calculations, chlorite in this association contains XMg from 0.5 to 0.505, which corresponds to that in the analyzed chlorite. Isopleths of the Si concentration in muscovite predicted by the model (3.04–3.15 apfu) are much lower than the ones observed in the sample (3.20–3.25 apfu). This discrepancy between the calculated and observed muscovite composition could be explained by the presence of paragonite in the fluid-sutured model that expands its stability field over that of albite (in the studied phyllite sample, we found only muscovite as having a low paragonite content, <6 mol%). Since the Si content in muscovite increases with pressure, we shall accept the upper limit of the stability field of muscovite–paragonite–chlorite–albite–calcite–quartz for estimating pressure. Chlorite XMg isopleths and chlorite thermometers constrain the temperature to 300–350 °C. The equilibrium mineral compositions calculated for water-saturated conditions are consistent with the natural compositions and define greenschist facies conditions at 300 °C and 3 kbar to 350 °C and 4 kbar.

Discussion

The metamorphic rocks from the area of the village of Klokotnitsa in the western Sakar unit contain sediment protoliths of varying composition and fossils of proven Triassic age (Čatalov 1961). Although generally similar in lithology and post-Triassic age metamorphism, these metasediments differ from the Triassic rocks of the eastern Sakar Unit by metamorphic grade, and in some aspects, by the provenance of sediment material. In the eastern Sakar Unit (Topolovgrad town area), Tzankova & Pristavova (2007) reported syn-kinematic peak metamorphic conditions of amphibolite facies (T = 536 to 658 °C, P = 3.5 to 8 kbar) for staurolite-garnet schists. A similar metamorphic grade in the range of 510–635 °C and 6–8 kbar was obtained for ortho- and para-amphibolites by Chavdarova & Machev (2017). The western Sakar Unit metasediments were affected by movements along the Maritza shear zone, that caused more complex deformation of the rocks. Although the lower metamorphic grade for the western metasediments is known from field studies and petrography (Kozhoukharov et al. 1968), we provide the first parameters for P–T conditions using a non-conventional approach.

Table 3: Representative feldspar analyses and structural formulae on the basis of 8 oxygen atoms from metasediments of the western Sakar Unit.

	TV-13a	TV-13a	TV-19	TV-19	TV-24	TV-34	TV-34	TV-34	TV-34	TV-34	TV-34
SiO_2	66.31	66.23	68.92	69.04	65.06	68.99	64.62	64.71	64.36	64.80	65.31
TiO_2	0.00	0.00	0.08	0.00	0.00	0.00	0.00	0.11	0.52	0.19	0.00
Al_2O_3	21.39	21.20	19.07	19.06	21.76	19.58	18.38	18.27	18.17	18.53	18.18
Fe_2O_3	0.00	0.00	0.19	0.06	0.71	0.00	0.00	0.41	0.00	0.00	0.00
MnO	0.00	0.00	0.00	0.03	0.00	0.00	0.10	0.01	0.00	0.01	0.17
MgO	0.00	0.00	0.00	0.00	0.00	0.00	0.00	0.00	0.00	0.00	0.00
CaO	0.10	0.19	0.07	0.08	0.46	0.33	0.16	0.11	0.09	0.12	0.00
Na_2O	12.20	12.38	11.69	11.67	11.83	11.09	0.37	0.68	0.24	0.49	0.07
K_2O	0.00	0.00	0.00	0.00	0.26	0.00	16.25	15.74	16.63	16.11	16.27
BaO	0.00	0.00	0.00	0.07	0.00	0.00	0.13	0.00	0.00	0.37	0.00
Total	100.00	100.00	100.02	100.01	100.08	99.99	100.01	100.04	100.01	100.62	100.00
Si	2.91	2.91	3.01	3.01	2.87	3.00	2.99	2.99	2.98	2.99	3.01
Ti	0.00	0.00	0.00	0.00	0.00	0.00	0.00	0.00	0.02	0.01	0.00
Al	1.11	1.10	0.98	0.98	1.13	1.01	1.00	1.00	0.99	1.01	0.99
Fe^{3+}	0.00	0.00	0.01	0.00	0.02	0.00	0.00	0.01	0.00	0.00	0.00
Sum T	4.02	4.01	4.00	4.00	4.02	4.01	4.00	4.00	4.00	4.00	4.00
Mg	0.00	0.00	0.00	0.00	0.00	0.00	0.00	0.00	0.00	0.00	0.00
Ca	0.01	0.01	0.00	0.00	0.02	0.02	0.01	0.01	0.00	0.01	0.00
Na	1.04	1.05	0.99	0.99	1.01	0.94	0.03	0.06	0.02	0.04	0.01
K	0.00	0.00	0.00	0.00	0.02	0.00	0.96	0.93	0.98	0.95	0.96
Sum A	1.04	1.06	0.99	0.99	1.05	0.95	1.00	0.99	1.01	1.00	0.96
Ab	1.00	0.99	1.00	1.00	0.96	0.98	0.03	0.06	0.02	0.04	0.01
An	0.00	0.01	0.00	0.00	0.02	0.02	0.01	0.01	0.00	0.01	0.00
Or	0.00	0.00	0.00	0.00	0.01	0.00	0.96	0.93	0.97	0.95	0.99

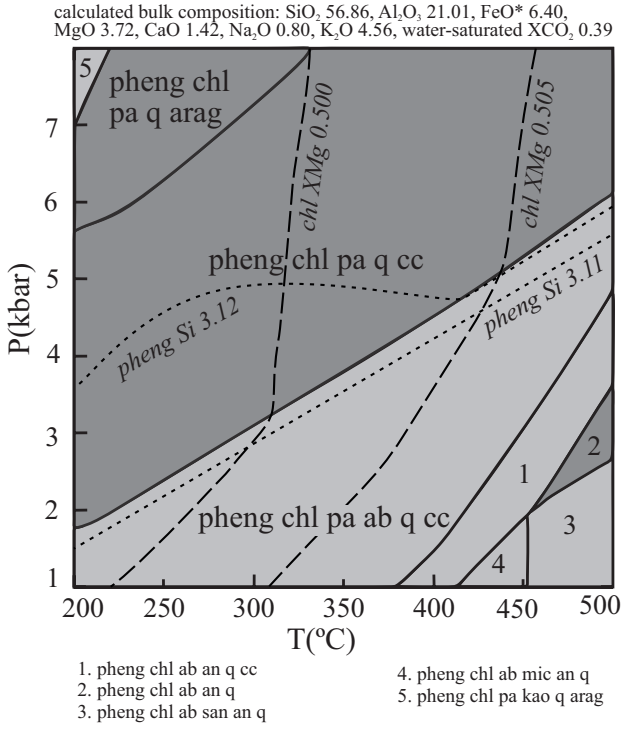

Fig. 5. Perple_X phase diagram calculated for sample TV-24 in the NCKFMASH–CO_2 system, water in excess, and XCO_2=0.39. The activity-composition models for the white mica and chlorite are of Holland & Powell (1998). Dashed lines are isopleths XMg in chlorite and dotted lines of Si [apfu] in muscovite.

The observed mineral associations correspond to greenschist facies and are in accordance with P–T estimates from chlorite thermometer and thermodynamic modelling (T=275–330 °C and P=3–4 kbar). Clastic metamorphic minerals, which record the higher-grade Variscan metamorphism, are lacking. Evidence of this older metamorphic event in the area is ambiguous due to the retrograde greenschist overprint. Single data of metamorphic Carboniferous zircon rims in Neproterozoic crust remnants were reported from the western Sakar Unit (Vladinova et al. 2017, 2020). Similar records in Early Carboniferous to Early Permian detrital zircons (Vladinova et al. 2018) were not found in the eastern Sakar Unit. These differences from both areas, together with the presence of Triassic magmatism (Bonev et al. 2021) in the western part and more abundant Cretaceous intrusions in the eastern part (Georgiev et al. 2012), emphasize the different tectonic settings and magmatic activity in both areas, which could explain the metamorphic gradient in the Sakar Unit. The difference in tectono–magmatic evolution is supported by geochronological studies of detrital zircons in siliciclastic metasediments as well, which suggest a different magmatic provenance source of sediment protoliths in both areas: Ordovician to Permian for the western Sakar Unit (Vladinova et al. 2017), and Early Carboniferous to Early Permian rocks for the eastern Sakar Unit (Vladinova et al. 2018).

Acknowledgements: This work was supported by the National Scientific Fund, project DN 14/5 2017.

References

Abad I., Nieto F., Guriérrez-Alonso G., Do Campo M., López-Munguira A. & Velilla N. 2006: Illitic substitution in micas of very low-grade metamorphic clastic rocks. *European Journal of Mineralogy* 18, 59–69. https://doi.org/10.1127/0935-1221/2006/0018-0059

Aysal N., Şahin S., Güngör Y., Peytcheva I. & Öngen S. 2018: Middle Permian–Early Triassic magmatism in the Western Pontides, NW Turkey: geodynamic significance for the evolution of the Paleo-Tethys. *Journal of Asian Earth Sciences* 164, 83–103. https://doi.org/10.1016/j.jseaes.2018.06.026

Bonev N., Filipov P., Raicheva R. & Moritz R. 2019: Timing and tectonic significance of Paleozoic magmatism in the Sakar unit of the Sakar-Strandzha Zone, SE Bulgaria. *International Geology Review* 61, 1957–1979. https://doi.org/10.1080/00206814.2019.1575090

Bonev N., Spikings R. & Moritz R. 2020: $^{40}Ar/^{39}Ar$ constraints for an early Alpine metamorphism of the Sakar unit, Sakar-Stranszha zone, Bulgaria. *Geological Magazine* 157, 2106–2112. https://doi.org/10.1017/S0016756820000953

Bonev N., Filipov P., Raicheva R. & Moritz R. 2021: Evidence of late Paleozoic and Middle Triassic magmatism in the Sakar-Strandzha Zone, SE Bulgaria, Regional geodynamic implications. *International Geology Review* 64, 1199–1225. https://doi.org/10.1080/00206814.2021.1917008

Bourdelle F. 2021: Low-temperature chlorite geothermometry and related recent analytical advances: A Review. *Minerals* 11, 130. https://doi.org/10.3390/min11020130

Bourdelle F. & Cathelineau M. 2015: Low-temperature chlorite geothermometry: a graphical representation based on a T–R^{2+}–Si diagram. *European Journal of Mineralogy* 27, 617–626. https://doi.org/10.1127/ejm/2015/0027-2467

Boyanov I., Kozhoukharov D., Goranov A., Ruseva M., Shiliafova G. & Yanev Y. 1989: Geological Map of Bulgaria. Scale 1:100 000. Haskovo Map Sheet. *Committee of Geology and Mineral Resources, Geology and Geophysics Corporation*.

Boyanov I., Kozhoukharov D., Goranov A., Yanev Y., Shiliafova G., & Ruseva M.1990: Geological Map of Bulgaria. Scale 1:100 000. Iskra Map Sheet. *Committee of Geology and Mineral Resources, Geology and Geophysics Corporation*.

Boyanov I., Goranov A., Shiliafova G., & Ruseva M. 1991: Geological Map of Bulgaria. Scale 1:100 000. Dimitrovgrad Map Sheet. *Committee of Geology and Mineral Resources, Geology and Geophysics Corporation*.

Boyanov I., Kozhoukharov D., Goranov A., Kozhoukharova E., Ruseva M. & Shiliafova G. 1992: Explanatory Note to the Geological Map of Bulgaria. Scale 1:100 000. Haskovo Map Sheet. *Committee of Geology, Department of Geophysical Prospecting and Geological Mapping*, 1–70 (in Bulgarian with English abstract).

Čatalov G. 1961: Triassische kristalline Schiefer und Magmagesteine zwischen Haskova und Dimitrovgrad. *Proceedings of the Bulgarian Academy of Sciences* 14, 503–506.

Cathelineau M. 1988: Cation site occupancy in chlorite and illites as a function of temperature. *Clay Minerals* 23, 471–485. https://doi.org/10.1180/claymin.1988.023.4.13

Cattò S., Cavazza W., Zattin M. & Okay A. 2017: No significant Alpine tectonic overprint on the Cimmerian Strandja Massif (SE Bulgaria and NW Turkey). *International Geology Review* 60, 513–529. https://doi.org/10.1080/00206814.2017.1350604

Chatalov G. 1990: Geology of the Strandza Zone in Bulgaria. *Geologica Balcanica, Series Operum Singulorum* 4. Sofia, BAS, Publishing House, 1–263 (in Bulgarian with English abstract).

Chavdarova S. & Machev Ph. 2017: Amphibolites from Sakar Mountain – geological position and petrological features. In:National Conference "Geosciences 2017" Sofia. *Bulgarian Geological Society*, 49–50.

Connolly D.A.J. 1990: Multivariable phase diagrams: an algorithm based on generalized thermodynamics. *American Journal of Science* 290, 666–718. https://doi.org/10.2475/ajs.290.6.666

Dabovski C. & Zagorchev I. 2009: Introduction: Mesozoic evolution and Alpine structure. In: Zagorchev I., Dabovski Ch. & Nikolov T. (Eds.): Geology of Bulgaria. Volume II. Part 5. Mesozoic Geology. *Prof. Marin Drinov Academic Publishing House*, Sofia, 13–37 (in Bulgarian with English summary).

Dabovski C., Boyanov I., Khrischev Kh., Nikolov T., Sapunov I., Yanev Y. & Zagorchev I. 2002: Structure and Alpine evolution of Bulgaria. *Geologica Balcanica* 33, 9–15.

Dimitrov S. 1958: Über die alpidische Regionalmetamorphose und ihre Beziehugen zu der Tektonik und dem Magmatismus in Sudostbulgarien. *Geologie* 7, 560–568.

Filipov P., Bonev N., Raicheva R., Chiaradia M. & Moritz R. 2018: Bracheting the timing of clastic metasediments and marbles from Pirin and Sakar Mts, Bulgaria: Implication of U–Pb geochronology of detritial zircon samples and $^{87}Sr/^{86}Sr$ of carbonate rocks. In: XXI International Congress of the GBGA. Salburg, 158.

Georgiev S., von Quadt A., Heinrich C., Peytcheva I. & Marchev P. 2012: Time evolution of rifted continental arc: Integrated ID-TIMS and LA-ICPMS study of magmatic zircons from the Eastern Srednogorie, Bulgaria. *Lithos* 154, 53–67.

Gerdjikov I. 2005: Alpine metamorphism and granitoid magmatism in the Strandja Zone: New data from the Sakar Unit, SE Bulgaria. *Turkish Journal of Earth Science* 14, 167–183.

Hey M.H. 1954: A new review of chlorites. *The mineralogy magazine and journal of the mineralogical society* 30, 278–292.

Holland B.H.T. & Powell R. 1998: An internally consistent thermodynamic data set for phases of petrological interest. *Journal of Metamorphic Geology*, 16, 309–343. https://doi.org/10.1111/j.1525-1314.1998.00140.x

Ivanov Zh. 2017: Tectonics of Bulgaria. *"St. Kliment Ohridski" Publishing House*, Sofia, 1–332 (in Bulgarian with English abstract).

Kozhoukharov D., Boyanov I. & Savov S. 1968: Geology of the region between village Klokotnitza and Maritza town, Haskovo district. In: Jubilee Geological Volume. *Geological Institute, BAS*, Sofia, 37–50 (in Bulgarian with German abstract).

Machev Ph., Ganev V. & Klain L. 2015: New LA–ICP–MS U–Pb zircon dating for Strandja granitoids (SE Bulgaria): Evidence for two-stage late Variscan magmatism in the internal Balkanides. *Turkish Journal of Earth Sciences* 24, 230–248. https://doi.org/10.3906/yer-1407-21

Makhloufi Y. & Samankassou E. 2019: Geochemical constrains on dolomitization pathways of the Upper Jurrasic carbonate rocks in the Geneva Basin (Switzerland and France). *Swiss Journal of Geosciences* 112, 579–596.

Massonne H.J. & Schreyer W. 1987: Phengite geobarometry based on the limiting assemblage with K-feldspar, phlogopite, and quartz. *Contributions to Mineralogy and Petrology* 96, 212–224. https://doi.org/10.1007/BF00375235

Okay A.I., Satır M., Tuysuz O., Akyuz S. & Chen F. 2001: The tectonics of the Strandja Massif: late-Variscan and mid-Mesozoic deformation and metamorphism in the northern Aegean. *International Journal of Earth Sciences* 90, 217–233. https://doi.org/10.1007/s005310000104

Peytcheva I., Georgiev S. & von Quadt A. 2016: U/Pb ID-TIMS dating of zircons from the Sakar Strandzha Zone: New data and old questions about the Variscan orogeny in SE Europe. In: National Conference "Geosciences 2016" Sofia. *Bulgarian Geological Society*, 71–72.

Pristavova S., Tzankova N., Gospodinov N. & Filipov P. 2019: Petrological study of metasomatic altered granitoids from Kanarata

Deposit, Sakar Mountain, southeastern Bulgaria. *Journal of Mining and Geological Sciences* 62, 53–61.

Rosen O., Desmons J. & Fettes D. 2007: Metacarbonate and related rocks. A systematic nomenclature for metamorphic rocks: 7. Metacarbonate and related rocks. A proposal on behalf of the IUGS Subcommission on the Systematics of Metamorphic Rocks. Recommendations. *IUGS Subcommission on the Systematics of Metamorphic Rocks*. https://www.ugr.es/~agcasco/personal/IUGS/pdf-IUGS/scmr_carb_r_metacarbonateandrelatedrocks.pdf

Sałacińska, A., Gerdjikov I., Gumsley A., Szopa K., Chew D., Gawęda A. & Kocjan I. 2021: Two stage of Late Carboniferous to Triassic magmatism in the Strandja Zone of Bulgaria and Turkey. *Geological Magazine* 158, 2151–2164 https://doi.org/10.1017/S0016756821000650

Sałacińska A., Gerdjikov Ia., Kounov A., Chew D., Szopa K., Gumsley A., Kocjan I., Marciniak-Maliszewska B. & Drakou F. 2022: Variscan magmatic evolution of the Strandja Zone (Southeast Bulgaria and Northwest Turkey) and its relationship to other Northe Gondwanan margin terranes. *Godwana Research* 109, 253–273. https://doi.org/10.1016/j.gr.2022.04.013

Schmid M., Fügenschuh S., Kounov B., Maţenco A., Nievergelt L., Oberhänsli P., Pleuger R., Schefer J., Schuster S., Tomljenović R., Ustaszewski K. & van Hinsbergen J.J.D. 2020: Tectonic units of the Alpine collision zone btween Eastern Alps ans western Turkey. *Godwana Research* 78, 308–374. https://doi.org/10.1016/j.gr.2019.07.005

Tzankova N. & Pristavova P. 2007: Metamorphic evolution of garnet-bearing schists from Sakar Mountain, Southeastern Bulgaria. *Comptes rendus de l'Académie bulgare des Sciences* 60, 271–278.

Vandeginste V. & John M.C. 2012: Influence of climate and dolomite composition on dedolomitization: insights from a multi-proxy study in the central Oman Mountain. *Journal of Sedimentary Research* 82, 177–195. https://doi.org/10.2110/jsr.2012.19

Vladinova Tz. & Georgieva M. 2020: New data on the westernmost part of the Sakar unit metamorphic basement, SE Bulgaria. In: National Conference "Geosciences 2020" Sofia. *Bulgarian Geological Society*, 105–107.

Vladinova Tz., Georgieva M. & Cherneva Z. 2017: U–Pb datting of detrital zircons from low-grade metasedimentary rocks in the Klokotnitsa village area, SE Bulgaria. In: National Conference "Geoscience 2017" Sofia. *Bulgarian Geological Society*, 67–68.

Vladinova Tz., Georgieva M., Bosse V. & Cherneva Z. 2018: U–Pb detrital zircons geochronology from metasedimentary rocks of the Sakar unit, Sakar-Strandzha zone, SE Bulgaria. In: National Conference "Geosciences 2018" Sofia. *Bulgarian Geological Society*, 67–68.

Vladinova Tz., Georgieva M. & Peytcheva I. 2019: U–Pb geochronology and geochemistry of rutiles from metaconglomerate in the Sakar–Strandzha zone, SE Bulgaria. In: National Conference "Geosciences 2019" Sofia. *Bulgarian Geological Society*, 91–93.

Zagorchev I. 2020: Geology of the Balkan Peninsula. Reference Module in Earth Systems and Environmental Sciences. In: Encyclopedia of Geology (Second Edition) 2021, 382–407. https://doi.org/10.1016/b978-0-08-102908-4.00056-4

Zagorchev I. & Budurov K. 2009: Triassic geology. In: Zagorchev I., Ch. Dabovski & T. Nikolov (Eds.): Geology of Bulgaria. Volume II. Part 5. Mesozoic Geology. *Prof. Marin Drinov Academic Publishing House*, Sofia, 39–130 (in Bulgarian with English summary).

Zane A.N. & Weiss Z. 1998: A procedure for classifying rock-forming chlorite based on microprobe data. *Rendiconti Lincei* 9, 51–56. https://doi.org/10.1007/BF02904455